Stochastic reaction-diffusion kinetics in the microscopic limit

David Fange[a], Otto G. Berg[b], Paul Sjöberg[a], and Johan Elf[c,1]

[a]Department of Cell and Molecular Biology, Uppsala University, 75124 Uppsala, Sweden; [b]Department of Molecular Evolution, Uppsala University, 75236 Uppsala, Sweden; and [c]Department of Cell and Molecular Biology, Science for Life Laboratory, Uppsala University, 75124 Uppsala, Sweden

Quantitative analysis of biochemical networks often requires consideration of both spatial and stochastic aspects of chemical processes. Despite significant progress in the field, it is still computationally prohibitive to simulate systems involving many reactants or complex geometries using a microscopic framework that includes the finest length and time scales of diffusion-limited molecular interactions. For this reason, spatially or temporally discretized simulations schemes are commonly used when modeling intracellular reaction networks. The challenge in defining such coarse-grained models is to calculate the correct probabilities of reaction given the microscopic parameters and the uncertainty in the molecular positions introduced by the spatial or temporal discretization. In this paper we have solved this problem for the spatially discretized Reaction-Diffusion Master Equation; this enables a seamless and physically consistent transition from the microscopic to the macroscopic frameworks of reaction-diffusion kinetics. We exemplify the use of the methods by showing that a phosphorylation-dephosphorylation motif, commonly observed in eukaryotic signaling pathways, is predicted to display fluctuations that depend on the geometry of the system.

diffusion-limited | mesoscopic | master equation | Smoluchowski | spatial

Both spatial and stochastic aspects of chemical reactions are important for the quantitative modeling of intracellular processes (1). Spatial, because diffusion is not sufficiently fast to make the system well-stirred between individual reaction events. Stochastic, because the number of reactants within diffusion range often is small, in which case the probabilistic and nonlinear nature of chemistry invalidates mean-field descriptions. There are two different basic theoretical frameworks describing spatially heterogeneous stochastic kinetics: the continuous microscopic framework (2–5) and the spatially discretized framework, here exemplified by the canonical reaction-diffusion (or multivariate) master equation (6, 7). The spatially and temporally continuous microscopic framework resolves the exact positions of molecules as well as the finest time scales of rapid reassociation after dissociation (5). The reaction-diffusion master equation (RDME), on the other hand, is coarse-grained and will be referred to as mesoscopic, as it conventionally averages out the kinetics at microscopic length and time scales. The RDME was developed to describe and analyze the influence of chemical noise in systems with many molecules and can be considered phenomenological in the sense that it is has not been derived from a microscopic model. In fact, the RDME has been shown to diverge and give unphysical results as the discretization approaches microscopic length scales (8, 9). This divergence is crucial because one way to ascertain that the chosen discretization is appropriate is to test that the results are invariant for a finer discretization. Due to the constraints on the spatial discretization, some combinations of reactions have not been possible to model using the RDME (10). In this paper we identify and resolve this inconsistency by embedding the microscopic description into the RDME framework. The derivation puts the RDME on a solid theoretical foundation and allows its use in a physically consistent transition from the microscopically resolved kinetics for pairs of molecules to mesoscopic systems with millions of molecules.

Models

The Microscopic Framework. The microscopic framework is based on the pioneering work by Smoluchowski (2) on irreversible diffusion-limited reactions and includes the extensions to more general diffusion-influenced (3, 4) and reversible (5) reactions. In this framework, molecules are treated as nonoverlapping spheres that diffuse as Brownian particles with diffusion rate D, in continuous space and time (*Methods*). When two reactants are at a distance corresponding to their reaction radius ρ they can bind with rate k. Bound molecules can split and dissociate back to the reaction radius with the microscopic rate γ at which point they can rapidly rebind on the sub-μs time scale or diffuse apart, with a probability that evaluates to $4\pi D\rho/(4\pi D\rho + k)$ (in three dimensions). The strength of the microscopic framework is that it can be used to calculate detailed kinetic properties for pairs of molecules (3, 5).

Unfortunately, the detailed analytical analysis is also restricted to pairs of molecules. However, using the Greens Function Reaction-Diffusion algorithm (GFRD) (11, 12), more complex reaction systems can be broken down to bimolecular interactions and individual realizations corresponding to multiparticle systems can be simulated in an exact and event-driven manner. However, GFRD, like any algorithm that resolves individual microscopic association-dissociation events, becomes very slow in the diffusion-limited regime with many molecules. As an alternative, several software packages have been developed to model and simulate stochastic biological reaction-diffusion systems as defined by individual molecules diffusing and reacting in continuous space [ChemCell (13), Smoldyn (14), MCell (15), STOCHSIM (16), etc.]. Unlike the GFRD algorithm, these methods sample the Brownian walk at regular time intervals Δt and then make a decision about which reactions occurred during the last time-step. The exact knowledge of the positions at certain time points may give an impression that the spatial information is very accurate in these methods. However, it is not known where the molecules have been in-between the sampled time points and the real spatial resolution is therefore limited to $\Delta x \approx \sqrt{(D\Delta t)}$ (14). In fact, there is no fundamental difference between a simulation method that is discretized in time or space. Either a molecule jumps a distance Δx after average time Δt or it jumps on average Δx after every Δt. The complicated part in both types of coarse-grained simulation scheme is to calculate the probability of the next reaction given the knowledge of the molecular positions and the uncertainty in these positions. In particular, the probability for reactions should correctly integrate the possible outcomes

of all the events that occur on a shorter length and time scale than what is explicitly modeled at the given discretization. For the temporally discretized methods there is no explicit formula for how the reaction probabilities should be calculated given the time-step and the parameters in the microscopic model; the same has—until now—been true for the spatially discretized schemes.

The Reaction-Diffusion Master Equation. In the RDME (6, 7), physical space is divided into subvolumes and the state of the system, $\mathbf{X} = \{X_{i,\mathbf{r}}\}$, is defined by the number of molecules, $X_{i,\mathbf{r}}$, of each species, i, in each subvolume, $\mathbf{r}$. In the subvolumes, the identities of the individual molecules are lost, which is appropriate when the molecules have time to diffuse throughout the subvolume and exchange position on the time scale on which reactions change the state of the system. The state changes when chemical reactions occur in a subvolume or when a molecule diffuses from a subvolume, $\mathbf{r}$, to one of its nearest neighbors, $\mathbf{r}'$. These events are considered elementary in the sense that they have a constant probability to occur in each infinitesimal time interval. The state description and the transition probabilities define a Markov process as described by the master equation (6)

$$\frac{dP(\mathbf{X})}{dt} = \sum_i D_i \left[\sum_{\mathbf{r},\mathbf{r}',X_{i,\mathbf{r}}} (X_{i,\mathbf{r}'} + 1)P(X_{i,\mathbf{r}'} + 1, X_{i,\mathbf{r}} - 1, \mathbf{X}, t) \right.$$
$$\left. - 2\omega X_{i,\mathbf{r}} P(\mathbf{X}, t) \right] + \sum_{\mathbf{X}'} \Psi(\mathbf{X}'; \mathbf{X}) P(\mathbf{X}', t)$$
$$- \sum_{\mathbf{X}'} \Psi(\mathbf{X}; \mathbf{X}') P(\mathbf{X}, t).$$

The first sum includes the first-order diffusion events, with rates D_i that depend on the spatial discretization and the translational diffusion constants; e.g., in a Cartesian mesh with lattice spacing ℓ, $D_i = D_i/\ell^2$. The first sum alone represents a random walk in discrete ω-dimensional space and continuous time. The remaining two sums describe the reaction events. Here, $\Psi(\mathbf{X}; \mathbf{X}')$ is the transition probability per unit time to go from state $\mathbf{X}$ to $\mathbf{X}'$, given that the system is in state $\mathbf{X}$. The RDME has for instance been used for analytical studies of spatial correlations in large nonequilibrium systems (7, 17). The general analytical approaches are, however, limited to relatively simple systems (18) and therefore a number of Monte Carlo simulation methods have been suggested (19, 20). Of these, the Next Subvolume Method (10) has been implemented in software packages MesoRD (21) and SmartCell (22) for simulation of biochemical reactions in cellular geometries.

In the conventional RDME, Ψ is simply taken to be the reaction rate evaluated for the concentrations in the individual subvolume (23), e.g., the transition probability associated with the association event $A + B \xrightarrow{k_a} C$ in three dimensions is taken to be $\Psi(\{X_{Ar}, X_{Br}, X_{Cr}\}, \{X_{Ar} - 1, X_{Br} - 1, X_{Cr} + 1\}) = k_a \Omega^{-1} X_{Ar} X_{Br}$, where X_{Ar} and X_{Br} are the numbers of A and B molecules in the subvolume $\mathbf{r}$ with volume Ω, and k_a is an intensive variable (e.g., the macroscopic reaction rate constant). However, as we will see $\Psi(\mathbf{X}; \mathbf{X}')$ can not be correctly calculated from the number of molecules in one subvolume alone and the rate constants both for association and dissociation necessarily need to be corrected for the size of the subvolumes. The scale-dependence is because the association process includes the diffusion from a random position in the subvolume before the reaction event and the dissociation process also includes the mixing in the subvolume after the dissociation event. This paper addresses the question of how the transition probability $\Psi(\mathbf{X}; \mathbf{X}')$ should be correctly calculated given the limited information about positions of the molecules at a specific discretization.

Results

The conventional approximation of the local reaction rates in RDME, Ψ, assumes that the molecules are well mixed in the subvolumes on the time scale of the reactions (24). However, this requirement cannot be met for the diffusion-influenced reactions of interest, since mixing without reacting is in general not possible. Therefore the diffusion aspect of the chemical reaction rates needs to be correctly accounted for in all discretized models, or different discretizations will correspond to different microscopic systems. For this reason we will in this paper derive the local probability of reaction given the state representation of the RDME based on the microscopic framework.

We begin by investigating the equilibration process for the bimolecular reaction $C \underset{k_a}{\overset{k_d}{\rightleftharpoons}} A + B$, when started with one C molecule in a finite three-dimensional volume or two-dimensional surface (Fig. 1). These reactions can be fully defined in the microscopic framework and we will stepwise translate them to the RDME framework. In the microscopic treatment (Fig. 1A), the C molecule can dissociate with the (microscopic) rate γ, which places the molecules at the distance of the reaction radius, ρ, apart. Without loss of generality, it is assumed that A is at the center of the coordinate system and B is diffusing in the region $r \in [\rho, R]$ with diffusion constant $D = D_A + D_B$. At the reaction radius the molecules can reassociate with the microscopic reaction rate constant k. This continuous model can be approximated by a RDME, where B makes memory-less diffusive jumps between shells of width h (Fig. 1B). In the innermost shell, $r \in [\rho, \rho + h]$ (volume V_1), A and B associate with rate $k_a V_1^{-1}$ and dissociate with rate $k_d = k_a/K$. In the conventional RDME treatment with fixed rate constants (k_a and k_d), the equilibration time, $T_{eq} = -\int_0^\infty t(dP_{bound}/dt)dt$, diverges at fine discretization (Fig. 2 A and B, black symbols). To overcome this problem we have derived
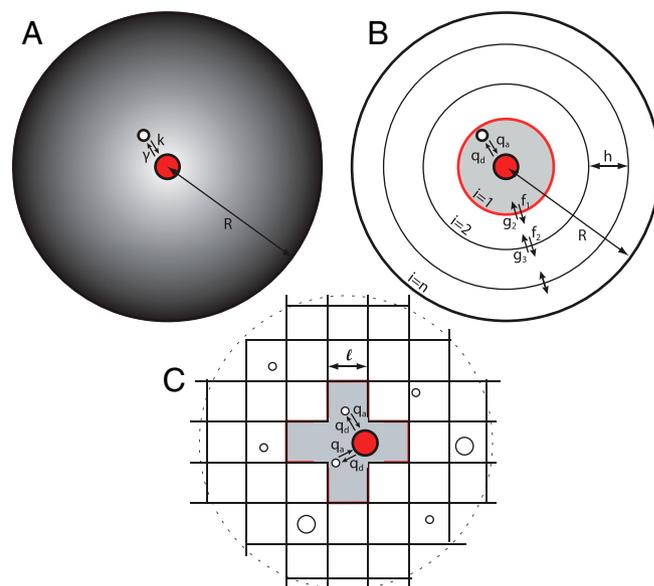
Fig. 1. A microscopically consistent transition to mesoscopic models. *A*. At the microscopic level, reactions are modeled by the reversible microscopic framework where molecules diffuse continuously in space and time and react at the reaction radius. *B*. In a master-equation description of the two-molecule system, space is discretized in concentric shells around one reactant (red). The other molecule (white) jumps between the shells in memory-less steps in continuous time. When in the inner shell the molecules react with the mesoscopic rate constants. Here q_a and q_d should be defined according to Eqs. **7** and **8** to be consistent with A. *C*. In a RDME model in Cartesian coordinates, a reactant (red) in the central subvolume can interact with molecules anywhere in the gray area with a rate constant corresponding to the united volume (area) of the gray regions.

Fig. 2. Approaching equilibrium in radial coordinates. The relaxation to steady state of the $C \rightleftharpoons A + B$ process in three dimensions (*A*) and two dimensions (*B*) for different discretizations (Fig. 1*B*; *n* is the total number of shells) is compared to the correct microscopic solution (solid line). In dimensionless variables $R = 100\rho$ and $D = R^2$, and the microscopic rate constant $k = \alpha 4\pi\rho D$ in three dimensions and $k = \alpha 2\pi D$ in two dimensions. In both cases the degree of diffusion control $\alpha = 100$ and the equilibrium constant, *K*, was chosen such that $P_{bound} = 0.01$ at equilibrium. *C,D*. The approximate mesoscopic rate constants given by Eqs. **1** and **2** (red circles) are compared to the rate constants that give the correct average relaxation time (solid line, Eqs. **7, 8**) for different degrees of diffusion control ($\alpha = 1$ and $\alpha = 100$).

exact expressions for how the association and dissociation rate constants scale with the spatial discretization, *h*, in order for the RDME to be consistent with the microscopic description (*Methods* Section). The scaled reaction rates $q_a(h)$ and $q_d(h)$, which replace k_a and k_d, will be considered mesoscopic because they span the range between the microscopic rate constants (*k* and γ) and the diffusion-influenced macroscopic rate constants defined in a large volume. In the parameter region of interest, i.e., $R > 10\rho$, the mesoscopic association rate constants can be accurately approximated (see Fig. 2 *C* and *D* and *SI Appendix*) by

$$q_a(h) = k/[1 + \alpha(1 - \beta)(1 - 0.58\beta)] \quad \text{in three dimensions} \quad [1]$$

$$q_a(h) = k/\{1 + \alpha \ln[1 + 0.544(1 - \beta)/\beta]\} \quad \text{in two dimensions.} \quad [2]$$

Here, $\beta = \rho/(\rho + h)$ is a unit-less measure for the spatial discretization, and $\alpha = k/4\pi\rho D$ in three dimensions and $\alpha = k/2\pi D$ in two dimensions is the degree of diffusion control. In both cases, the dissociation rate constant $q_d(h)$ is simultaneously determined by the constant ratio $q_a(h)/q_d(h) = K$ as required by microscopic reversibility. Fig. 2 *C* and *D* show the excellent agreement between these approximate rate constants (Eqs. **1, 2**) and the exact values (Eqs. **7, 8**) required to give the same equilibration time as the reversible microscopic model.

At fine discretization ($h \to 0$, i.e., $\beta \to 1$), where the diffusion part is handled exclusively by the diffusive jumps between subvolumes, the mesoscopic reaction rates approach the microscopic ones: $q_a \to k$ and $q_d \to \gamma = k/K$. In three dimensions, at coarse discretization ($h > 10\rho$, i.e., $\beta \ll 1$), many microscopic models converge and the mesoscopic rate constants can be accurately described by the macroscopic diffusion-influenced ones, $k_a = k/(1 + \alpha) = 4\pi D\rho k/(4\pi D\rho + k)$ and $k_d = \gamma/(1 + \alpha) = 4\pi D\rho\gamma/(4\pi D\rho + k)$. In two dimensions however, there are no limiting values for q_a and q_d with increasing *h* (decreasing β) and the

mesoscopic rate constants keep decreasing for coarser discretization; thus, in principle, the rate constants in two dimensions will have to be corrected on all length scales. When the mesoscopic rate constants are used in the RDME (red symbols in Fig. 2 *A* and *B*) no deviations from the microscopic model can be observed at fine discretization.

In making the transition to Cartesian coordinates (lattice size ℓ), it is not obvious which length scale, *h*, should be used to calculate $q(h)$. The choice of *h*, however, should reflect the uncertainty in distance between possible reaction partners for a given discretization. In the radial coordinates the central *A*-molecule is equally likely to react with any *B*-molecule in the inner shell of radius $h + \rho$ (gray region in Fig. 1*B*). Using the same principle in Cartesian coordinates, we define *h* from the region where an *A* molecule can find reaction partners without making a diffusive jump. However, we need to account for the fact that two reactants can be in neighboring subvolumes. We solve this problem by discretizing space at a resolution twice as fine as the one used to calculate the reaction probabilities, such that *A* molecules in one subvolume can interact with *B* molecules also in neighboring subvolumes (Fig. 1*C*). The reaction volume for which the *B* molecule concentration is calculated is therefore the union of the central subvolume and its neighbors; thus, the length scale *h* is calculated from $4\pi(h + \rho)^3/3 = 7\ell^3$ in three dimensions and $\pi(h + \rho)^2 = 5\ell^2$ in two dimensions. In this way the geometry with a central molecule surrounded by a reaction volume is retained from the radial description. It may seem that we cannot assume that the *A* molecule is uniformly surrounded by *B* molecules if it is known that they are in neighboring subvolumes and that the assumptions used when deriving $q(h)$ in radial coordinates therefore would break down. However, the localization in a discretized description cannot be known to a higher precision than twice the sampling unit (Nyquist-Shannon theorem), which in our case corresponds to the fact that the elementary diffusive jumps also include mixing in the receiving subvolume. For this reason, there is no need to assume an initial displacement between molecules in neighboring subvolumes. In Fig. 3 we show that the two-particle system from Fig. 2 in this way can be accurately modeled in Cartesian coordinates all the way down to lattice sizes corresponding to the size of the reactants, i.e., $\ell \sim 2\rho$.

Discussion

All theoretical frameworks in physics have a limited range of validity; however, it is desired that this range is as large as possible and that it is consistent with other descriptions in the appropriate limits. For instance, it can be shown that the RDME converges to

Fig. 3. Cartesian discretization requires twice as fine resolution in three dimensions (*A*) and in two dimensions (*B*). Comparison of simulated relaxation kinetics based on reaction rates calculated for individual subvolumes (black symbols) or including also nearest neighbors (red symbols). Unless reactions between molecules in neighboring subvolumes are included, many diffusion-limited reaction events will be unaccounted for in simulations. For this reason the conventional treatment where reactions are confined to individual subvolumes (black symbols) will lead to too slow relaxation kinetics. However, if the spatial discretization is made twice as fine and molecules are allowed to react also between neighboring subvolumes, the RDME model is in excellent agreement with the microscopic description (red symbols compared to black line).

the macroscopic description of reaction-diffusion kinetics when many molecules are in diffusion range between consecutive reactions (25). However, in the other limit the RDME has not been consistent with the microscopic picture, especially not for reversible reactions for which detailed balance has to be strictly obeyed at all length scales (8, 9).

Nonequilibrium Steady States. As we have seen, the spatial discretization of the conventional RDME changes the kinetics of the system, but not the equilibrium point. However, in nonequilibrium situations, changes in kinetics of individual reactions typically lead to changes also in the steady state. To exemplify this phenomenon we use a multiparticle system where there is a net flux through the dimerization reaction:

$$A + B \underset{k_d}{\overset{k_a}{\rightleftharpoons}} C, \qquad \varnothing \overset{k_1}{\rightarrow} C, \qquad A \overset{k_2}{\rightarrow} \varnothing, \qquad B \overset{k_2}{\rightarrow} \varnothing. \qquad [3]$$

The introduction of a zeroth order irreversible birth event and irreversible first-order decay events are straight forward, because they do not depend on the spatial correlations between molecules. There is, however, a big difference between the reversible first-order dissociation event and a first-order decay event. The former depends on a number of microscopic reassociation events and therefore also on the discretization, whereas the latter, by definition, does not. In Fig. 4 we see how the copy number of C depends on the spatial discretization in both three dimensions and two dimensions unless the mesoscopic, scale-dependent, rate constants are used. The concentration of C molecules in the macroscopic steady state of [3] is given by $C = k_1/k_d + K(k_1/k_2)^2$. This steady state is also given by the mesoscopic simulations in three dimensions (Fig. 4A), as long as k_2 is slow

Fig. 4. Classical treatment results in discretization-dependent steady states both in three dimensions (*A*) and two dimensions (*B*). In a conventional lattice-based treatment the rates of diffusion-limited reactions does not depend on the spatial discretization and the steady state of a nonequilibrium system will therefore incorrectly change with the lattice spacing. Here, we show the mean number of C molecules from 100 simulations of [3] in a cube with side length, $L_c = 100\rho$ (*A*) and a quadratic plane with side length, $L_p = 1,000\rho$ (*B*). Note that the number of C molecules, at steady state, increases with finer discretization using the conventional lattice-based treatment with macroscopic rate constants calculated in individual subvolumes (dashed lines). On the other hand, when the mesoscopic rate constants, given by equations and are used, there is practically no difference between the steady-state number of C molecules using different discretizations (solid lines). Mesoscopic association rate constants $q_a(\ell)$ (solid lines) are calculated using the microscopic rate constant $k = \alpha 4\pi\rho D$ in three dimensions and $k = \alpha 2\pi D$ in two dimensions, including nearest neighbors as in Fig. 3. The degree of diffusion control is $\alpha = 100$. The diffusion rate, $D = L_c^2$ in three dimensions and $D = 10^{-2}L_p^2$ in two dimensions. The equilibrium constant is $K = q_a/q_d = 10^{-2}L_c^3$ in three dimensions and $K = q_a/q_d = 10^{-2}L_p^2$ in two dimensions. The macroscopic association rate constant in three dimensions is calculated as $k_a = 4\pi\rho D\alpha/(1 + \alpha)$. In two dimensions a corresponding macroscopic rate constant is not well defined and here we use simply $k_a = 2\pi D\alpha/(1 + \alpha)$ to show the effect of using a scale-independent rate. The equilibrium constant is the same as for the mesoscopic case. The synthesis rate constant for production of C molecules is $k_1 = 600L_c^{-3}$ in three dimensions and $k_1 = 180L_p^{-2}$ in two dimensions. The first-order rate constant for decay of A and B is $k_2 = 10$.

compared to the microscopic rebinding events. However, in two dimensions, the macroscopic diffusion-limited rate constants (k_a and k_d) are scale dependent at all scales and macroscopic steady-state levels cannot be directly calculated in this way. Therefore, a consistent description of the macroscopic behavior in two dimensions can be provided only by the mesoscopic simulations (Fig. 4B). In this system, [3], the coarsest discretization used in Fig. 4 are sufficient. In the general case, however, the required discretization depends on the system (e.g., Fig. 5 below), as discussed further in the *SI Appendix: Fig. S3*.

Bridging Microscopic and Mesoscopic Simulations. Different kinds of biochemical processes require different levels of spatio-temporal resolution to capture the central features. An important demarcation is between systems where the microscopic rebinding events between two molecules need to be resolved in order to correctly calculate the probabilities of other events (26), and systems where the microscopic states can be embedded in a more or less coarse-grained model where the outcome of the microscopic interaction between pairs of molecules have been correctly averaged out. An example of the latter is the case of reversible binding of proteins to DNA which includes many microscopic dissociation events, but in most cases can be modeled with macroscopic average rates in the coarse-grained states of bound and free (27, 28). One case where the microscopic events actually are critically important for the overall properties of a biological system is the commonly occurring two-step phosphorylation- dephosphorylation cycle described in Fig. 5A (29). In a recent investigation it was demonstrated that the sensitivity in phosphorylation state to the kinase/phosphatase ratio is compromised if the enzymes act processively due to diffusion-controlled microscopic rebinding to the product of the previous reaction (12). This truly microscopic phenomenon with macroscopic implications was originally analyzed using GFRD, but can now also be accurately accounted for in the RDME framework at fine discretization (Fig. 5B). However, the phenomenon disappears if modeled at too large spatial (or temporal) discretization because the dissociation event in that case necessarily includes partial diffusion away from the product (see Fig. 5B).

There are however many cases where the microscopic association-dissociation between pairs of molecules at the *ns* time scale is not important for the overall properties of the system, although the stochastic outcome of these interactions and the spatially heterogeneous distributions of molecules are important. In these cases it is advantageous to use a coarse-grained alternative to GFRD, because it makes it possible to simulate larger systems with more molecules. For instance, in the nonprocessive and sensitive parameter regime of the phosphorylation example above, we expanded the system 250 times while maintaining the concentrations of molecules. Here, we find that the geometry of the three-dimensional volume strongly influences the local fluctuations in the number of molecules. In a cubic geometry the Fano factor (variance over mean) is close to unity at all length scales. However, in a stretched-out three-dimensional geometry (cuboid) of the same volume, the Fano factor starts near the Poission limit for short distances, then reaches a maximum at a characteristic length scale and then goes back down to one when averaged over the whole system (Fig. 5D). This phenomenon corresponds to noise-induced spatial domains where molecules of the same state of phosphorylation cluster (Fig. 5C). Similar phenomena have previously been described for bistable modification cycles (10) but not for the supposedly more common monostable motifs. Because the doubly phosphorylated species typically regulates the downstream process in a nonlinear manner, such as in a MAPK cascade, the activity of the downstream processes will depend on the whole distribution of the fluctuations and not only on the average value (30). For this reason, we predict that the overall activity of sensitive signal transduction cascades will depend on
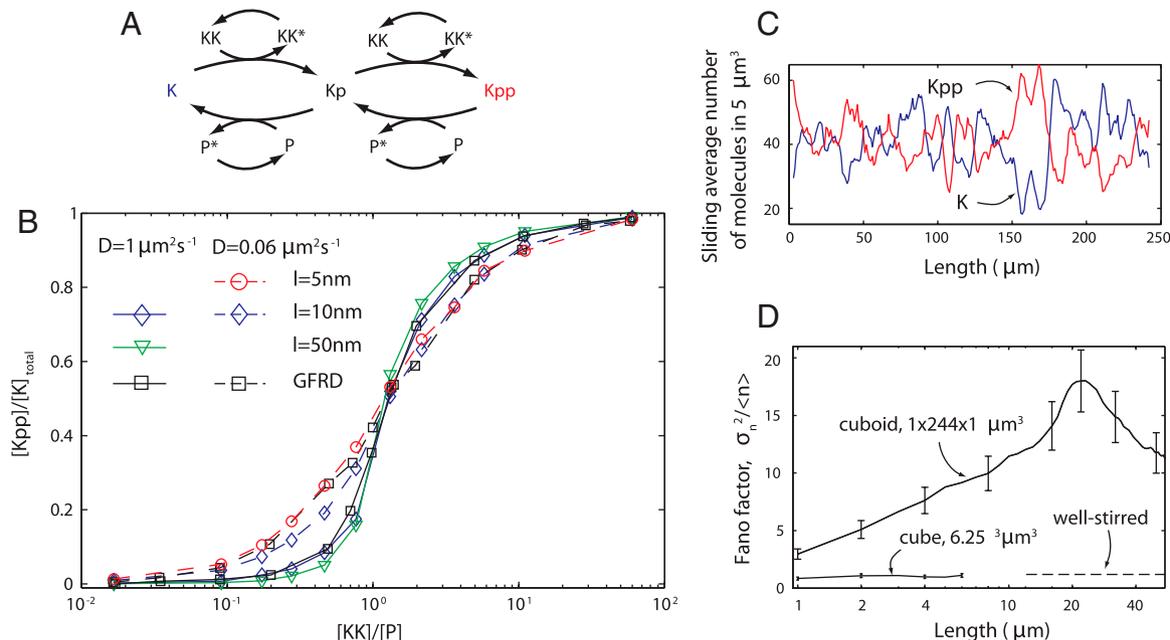
Fig. 5. RDME treatment of the MAPK motif gives identical results as the microscopic treatment and also displays geometry-dependent noise. The MAPK motif in (A) requires a spatial discretization of the size corresponding to the reaction radius to reproduce the microscopic treatment by ref. 12. The effect of this requirement is shown in (B) where the RDME analysis is compared to the results of GFRD. In the case of slow diffusion ($D = 0.06$ $\mu m^2 s^{-1}$) microscopic rebinding events are important and a fine discretization (5 nm) is needed to resolve these. When diffusion is faster ($D = 1$ $\mu m^2 s^{-1}$) the mechanism is distributed and a coarse discretization (50 nm) is possible. The parameters are the same as in ref. 12. When the system from (B), using $D = 1$ um^2 s^{-1} and $[KK]/[P] = 1$, is scaled up 244 times, the fluctuations in the number of molecules depend on the geometry. When the reactions are put into a cuboid of size $1 \times 244 \times 1$ um, there will be transient domain separation of K and Kpp as shown in (C). Here we display a snapshot of the number of molecules per 1 um^3 calculated as a sliding average over a 5 μm window. In (D) the Fano factors on different length-scales are compared between the cuboid (upper curve) and a cube (lower curve) of the same volume. The fano factor on the y-axis is calculated for the total number molecules in boxes of size $1 \times 1 \times i$ μm^3, where i is given by the x-axis. The fano factor of the cube is also compared to a well stirred, i.e. nonspatial, stochastic treatment (dashed line). The fano factor is calculated at 20 s of 100 simulations started close to the steady state. Simulations used in (C) and (D) use subvolumes with side-length 250 nm.

the geometry of the three-dimensional volume, as long as the downstream process responds to the local and not the global concentration of phosphorylated molecules. This phenomenon would be a direct spatial analogue of the stochastic-focusing phenomena that previously have been described for fluctuations in well-stirred systems (30).

In summary, all spatially or temporally discretized reaction schemes will result in inconsistent and misleading reaction-diffusion models unless the scale dependence of the association and dissociation rate constants is duly accounted for. For the spatially discretized models we have solved the problem by using the microscopically consistent derivation of the rate constants, which allows for a seamless and physically justified transition from microscopic to coarse-grained models in two dimensions and three dimensions. The result also makes it possible to use a spatial discretization that is correct for all reactions in a multireaction system, something that previously was problematic considering the different discretization requirements for different reactions (10). Similarly, it should be possible to derive temporally discretized simulation schemes for microscopically defined systems that can handle reactions with different degrees of diffusion control. The present formulation of the RDME can be used to develop new numerical algorithms and simulation tools for physically consistent analysis of chemical fluctuations in biological processes. Such tools will be necessary to analyze fluctuations and geometry-dependent properties of systems similar to those here found in the dual phophorylation system.

Methods

Here we will summarize the results of the full derivations given in the *SI Appendix*.

In the microscopic model (Fig. 1A), let $p(r,t)$ denote the probability density for the ligand to remain unbound and separated from the target center by distance r at time t and $p_b(t)$ the probability for the ligand to be bound at time t. The time evolution of the system is then determined by

$$\frac{\partial p(r,t)}{\partial t} = D \frac{1}{r^{\omega-1}} \frac{\partial}{\partial r}\left(r^{\omega-1}\frac{\partial p(r,t)}{\partial r}\right), \qquad \frac{dp_b(t)}{dt} = kp(\rho,t) - \gamma p_b(t),$$

[4]

where k is the microscopic association rate constant, γ is the microscopic dissociation rate constant, D is the diffusion rate constant, and $\omega = 1, 2, 3$ is the dimensionality. The microscopic rate constants are defined by the boundary condition of the diffusion equation at the interface $r = \rho$, $\theta_\omega \rho^{\omega-1} D \partial p(r,t)/\partial r|_{r=\rho} = kp(\rho,t) - \gamma p_b(t)$, where $\theta_1 = 1$, $\theta_2 = 2\pi$, and $\theta_3 = 4\pi$. The outer boundary, $r = R$, is reflective, such that $\partial p(r,t)/\partial r|_{r=R} = 0$.

In the master-equation approach, the domain is discretized in r by n shell-shaped volumes using the step size h, Fig. 1B. Reactions occur only in the innermost shell. Let $p_j(t)$ be the probability for the ligand to be unbound in the volume where $r \in [\rho + (j-1)h, \rho + jh]$. Then the master-equation approximation of Eq. 4 can be written

$$\frac{dp_b(t)}{dt} = \frac{q_a}{V_1}p_1(t) - q_d p_b(t),$$

$$\frac{dp_1(t)}{dt} = g_2 p_2 - f_1 p_1 + q_d p_b(t) - \frac{q_a}{V_1}p_1(t),$$

$$\frac{dp_i(t)}{dt} = g_{i+1}p_{i+1} - (g_i + f_i)p_i + f_{i-1}p_{i-1},$$

$$\frac{dp_n(t)}{dt} = -g_n p_n + f_{n-1}p_{n-1},$$

[5]

where $i = 2, \ldots, n-1$, $f_j = D\omega \frac{r_j^{\omega-1}}{h(r_j^\omega - r_{j-1}^\omega)}$, $g_j = D\omega \frac{r_{j-1}^{\omega-1}}{h(r_j^\omega - r_{j-1}^\omega)}$, $r_j = \rho + jh$, and V_1 is the available volume of the innermost subvolume, that is $V_1 = (\theta_\omega/\omega)[(\rho + h)^\omega - \rho^\omega]$.

For a system starting in the bound state, the equilibration time in the microscopic model can be calculated as

$$T_{eq} = -\int_0^\infty t \frac{dp_b(t)}{dt} dt = \int_0^\infty [p_b(t) - p_b^{eq}] dt$$
$$= p_b^{eq}(1 - p_b^{eq})T_{bind}. \qquad [6]$$

$p_b^{eq} = K/(K+V)$ is the probability of binding at equilibrium, with the binding constant $K = k/\gamma$, and T_{bind} is the mean time for irreversible binding given a uniform initial distribution of the free molecule. In two dimensions and three dimensions one finds $T_{bind} = [1 + \alpha F(\lambda)]V/k$ where the function $F(\lambda)$ is given by

$$F^{2D} = [4\ln(1/\lambda) - (1 - \lambda^2)(3 - \lambda^2)]/4(1 - \lambda^2)^2 \quad \text{and}$$
$$F^{3D} = (1 - \lambda)(5 + 6\lambda + 3\lambda^2 + \lambda^3)/5(1 + \lambda + \lambda^2)^2.$$

Here, $\lambda = \rho/R$ in all expressions while α is the extent of diffusion control: $\alpha = k/2\pi D$ in two dimensions and $\alpha = k/4\pi D\rho$ in three dimensions. V is the available diffusion volume appropriate for two dimensions and three dimensions.

The mesoscopic rate constants q_a and q_d are calculated such that the equilibration time is the same in the master equation as in the microscopic model. The solution can be expressed as

$$\frac{q_a}{k} = \left\{ 1 + \alpha \left[F^{2D}(\lambda) - (1 - \lambda)\frac{1}{n}\sum_{i=1}^{n-1} \frac{(A_{i+1}^{2D})^2}{\lambda + i(1-\lambda)/n} \right] \right\}^{-1}$$

in two dimensions   [7]

$$\frac{q_a}{k} = \left\{ 1 + \alpha \left[F^{3D}(\lambda) - \lambda(1 - \lambda)\frac{1}{n}\sum_{i=1}^{n-1} \left(\frac{A_{i+1}^{3D}}{\lambda + i(1-\lambda)/n} \right)^2 \right] \right\}^{-1}$$

in three dimensions.   [8]

Here, A_j is the total volume of the shells from j up to n relative to the total free volume, such that $A_1 = 1$. In Fig. 2 C and D, the exact expressions for the rate constants Eqs. 7 and 8 are compared to the excellent, and more informative, approximations given by Eqs. 1 and 2. The mesoscopic dissociation rates are simultaneously given by $q_a/q_d = k/\gamma = K$, as required by microscopic reversibility, in both two dimensions and three dimensions.

1. Di Ventura B, Lemerle C, Michalodimitrakis K, Serrano L (2006) From in vivo to in silico biology and back. *Nature* 443:527–533.
2. von Smoluchowski M (1917) Versuch eine mathematischen theorie der koagulationskinetik kolloidaler losungen. *Zeitschrift für physikalische Chemie* 92:129–168.
3. Noyes RM (1961) Effects of diffusion rates on chemical kinetics. *Progress in Reaction Kinetics* 1:129–160.
4. Collins FC, Kimball GE (1949) Diffusion-controlled reaction rates. *Journal of Colloid Science* 4:425–437.
5. Berg OG (1978) On diffusion-controlled dissociation. *Chem Phys* 31:47–57.
6. Nicolis G, Prigogine I (1977) *Self-organization in nonequilibrium systems* (John Wiley & Sons, New York).
7. Gardiner C, Mc Neil K, Walls D, Matheson I (1976) Correlations in stochastic theories of chemical reactions. *J Stat Phys* 14:307–331.
8. Isaacson S (2008) Relationship between the reaction-diffusion master equation and particle tracking models. *J Phys A-Math Theor* 41:065003.
9. Erban R, Chapman J (2009) Stochastic modelling of reaction-diffusion process: alorithms for bimolecular reactions. *Phys Biol* 6:046001.
10. Elf J, Ehrenberg M (2004) Spontaneous separation of bi-stable biochemical systems into spatial domains of opposite phases. *Syst Biol* 1:230–236.
11. van Zon JS, ten Wolde PR (2005) Simulating biochemical networks at the particle level and in time and space: Green's function reaction dynamics. *Phys Rev Lett* 94:128103.
12. Takahashi K, Tanase-Nicola S, ten Wolde PR (2010) Spatio-temporal correlations can drastically change the response of a MAPK pathway. *Proc Natl Acad Sci USA* 107:2473–2478.
13. Plimpton S, Slepoy A (2005) Microbial cell modeling via reacting diffusive particles. *J Phys Conf Ser* 16:305–309.
14. Andrews SS, Bray D (2004) Stochastic simulation of chemical reactions with spatial resolutionand single molecule detail. *Phys Biol* 1:137–151.
15. Stiles J, Bartol T (2001) Monte Carlo methods for simulating realistic synaptic microphysiology using MCell. *Computational neuroscience: Realistic modeling for experimentalists*, ed DS Erik (CRC Press, Boca Raton, FL), pp 87–127.
16. Le Novère N, Shimizu TS (2001) STOCHSIM: modelling of stochastic biomolecular processes. *Bioinformatics* 17:575–576.
17. Nicolis G, Malek Mansour M (1984) Onset of spatial correlations in nonequilibrium systems: a master-equation description. *Phys Rev A* 29:2845 2853.
18. Tauber U, Howard M, Vollmayr-Lee B (2005) Applications of field-theoretic renormalization group methods to reaction–diffusion problems. *J Phys A-Math Gen* 38:79–131.
19. Breuer HP, Huber W, Petruccione F (1996) Fast Monte Carlo algorithm for nonequilibrium systems. *Phys Rev E* 53:4232–4235.
20. Blue JL, Beichl II, Sullivan F (1995) Faster Monte Carlo simulations. *Phys Rev E* 51:R867–R868.
21. Hattne J, Fange D, Elf J (2005) Stochastic reaction-diffusion simulation with MesoRD. *Bioinformatics* 21:2923 2924.
22. Ander M, et al. (2004) SmartCell, a framework to simulate cellular processes that combines stochastic approximation with diffusion and localization: Analysis of simple networks. *Syst Biol* 1:129 138.
23. Gardiner C (1985) *Handbook of stochastic methods* (Springer-Verlag, Berlin), Second Ed.
24. Baras F, Mansour MM (1997) Microscopic simulation of chemical instabilities. *Adv Chem Phys* 100:393–475.
25. Arnold L, Theodosopulu M (1980) Deterministic limit of the stochastic model of chemical reactions with diffusion. *Adv Appl Probab* 12:367–379.
26. Berg OG, Ehrenberg M (1983) *Biophys Chem* 17:13–28.
27. van Zon JS, Morelli MJ, Tanase-Nicola S, ten Wolde PR (2006) Diffusion of transcription factors can drastically enhance the noise in gene expression. *Biophys J* 91(12):4350–4367.
28. Berg OG, Winter RB, von Hippel PH (1981) Diffusion-driven mechanisms of protein translocation on nucleic acids. 1. Models and theory. *Biochemistry* 20:6929–6948.
29. Markevich NI, Hoek JB, Kholodenko BN (2004) Signaling switches and bistability arising from multisite phosphorylation in protein kinase cascades. *J Cell Biol* 164:353–359.
30. Paulsson J, Berg OG, Ehrenberg M (2000) Stochastic focusing: fluctuation-enhanced sensitivity of intracellular regulation. *Proc Natl Acad Sci USA* 97:7148–7153.

BIOPHYSICS AND COMPUTATIONAL BIOLOGY

CHEMISTRY